How to cite this article:
Authors: Wit Grzesik
Title of article: „ Progress in modelling and simulation of the machining process – part II: Mesh-free modeling and simulation"
Mechanik, No. 5–6 (2024)
DOI: https://doi.org/10.17814/mechanik.2024.5-6.9

Progress in modelling and simulation of the machining process – part II: Mesh-free modeling and simulation

WIT GRZESIK *

DOI: https://doi.org/10.17814/mechanik.2024.5-6.9

* Prof. dr hab. inż. Wit Grzesik – wit.grzesik@gmail.com, https://orcid.org/0000-0003-3898-5119 – Opole, Polska

In this paper some rules of mesh-free/meshless modeling and numerical simulations of fundamental physical phenomena associated with the machining process, including mechanisms of plastic deformation, chip formation and interfacial friction are overviewed. Some representative examples of the mesh-free modeling application to material removal processes at different scales, i.e. machining processes, water-jet assisted processes, additive machining processes and simulation of micromachining processes using commonly used SPH (smoothed particle hydrodynamics) method are given.
KEYWORDS: mesh-free modeling, numerical simulations, machining process

Introduction

In the last decade, there has been a growing interest in the use of the so-called meshless modelling and simulation of additive and material forming processes, which is a consequence of the development of graphical modelling methods performed using graphics cards, i.e. on one processor (CPU) and graphical solvers, i.e. on many processors (GPU) [1–4]. The previous article [1] described the use of the MD (molecular dynamics) and SPH (smoothed particle hydrodynamics) in hybrid modelling of the cutting process combining traditional mesh modelling (FEM/FEM, but mainly the hybrid FEM Eulerian-Lagrangian method – ALE), which is one of the methods of implementing the so-called large-scale modelling. In this way, their numerous applications in modelling and simulation in solid mechanics, soil mechanics, multiphase flows, casting (solidification) and welding processes and analysis of structures for modelling and simulation of machining processes are expanded [5, 7, 8, 16].

Chronologically, the first meshless method should be considered the molecular dynamics method, which was already used in the 1980s to model and simulate the cutting process in the micro and nanoscale [6]. The basic meshless methods include the discrete element method (DEM) and the SPH method called smoothed particle hydrodynamics, the smoothed particle hydrodynamics method, or the fuzzy/smoothed particle method.

The basic difference is the fact that in meshless methods, the computational domain does not have to have explicitly defined external boundaries, which means that the size of the domain depends on the current location of the objects taking part in the simulation. Alternatively, one can specify the maximum external boundaries, beyond which the object stops taking part in the simulation. It should be noted that in computer mechanics, there are over 40 different meshless methods and varieties based on different classification criteria [7]. The most frequently used methods in the aforementioned manufacturing processes include the meshless finite difference method (MFDM), the free element Galerkin (EFG), finite point method (FPM), which are based on the local approximation method of weighted moving least squares (MWLS) and the basic SPH method based on the integral kernel approximation [7]. SPH uses the kernel approximation from the so-called kernel function, which can be interpreted as a kind of weighting function. In contrast to the mesh methods, a set of arbitrarily

distributed nodes is given, which are not connected by any structure (element, mesh type) and which can be arbitrarily removed, moved, and even new nodes can be added to them. The SPH method gave rise to other methods from the family of meshless methods, e.g. such as Element-Free-Galerkin (EFG) or Meshless Local Petrov-Galerkin Methods (MLPG), however both EFG and MLPG require discretization in the form of a kind of grid (background mesh) in order to perform integration, due to which they partially lost the greatest advantage of e.g. SPH, i.e. the ability to describe large deformations and fragmentation.

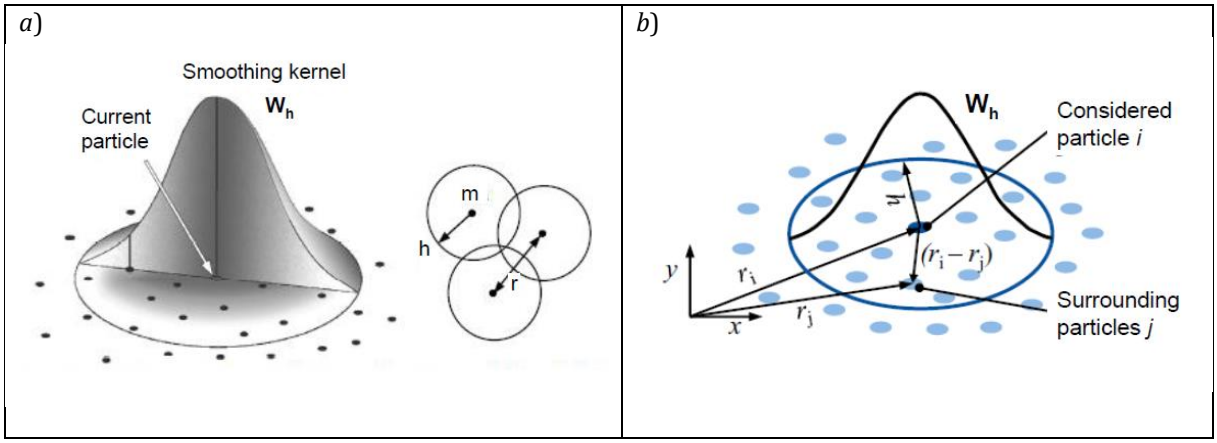

Fig. 1. Exemplary diagram of smoothing kernel function $W_h(r)$ in R^3 space (*a*) and the sphere of its influence (*b*). Symbols: *m* – mass, *r* – distance between particles, *h* – smoothing length [8, 10, 25]

The parameter h is called the smoothing length, which determines the distance at which a particle can interact with other particles. Most often in a simulation it remains constant throughout the computation. The smoothing function depends on the smoothing length h and the distance $(r_i - r_j)$ – usually equal to $2h$, of the considered particle from the surrounding particles as in fig. 1*b*. The approximation kernel/weight function (W_h) can be, for example, a Gaussian function (fig. 1), a quadratic function or a cubic *B*-spline function of the third degree or a special function of the fourth degree. The smoothing length h can be related to the radius of the kernel function carrier (r), while the number of SPH particles in a given function carrier (N_N) governs the accuracy of the approximation [8, 10, 19]. It is only necessary to take into account that there is an appropriate number of neighbours within the radius . This number should range from $N_N/2$ to N_N.

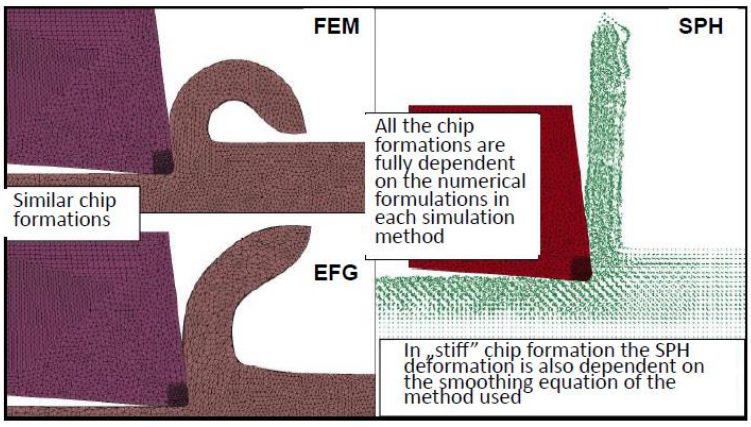

Fig. 2. Comparison of chip formation using FEM, EFG and SPH methods [9]

Figures 2, 3 and 4 compare the simulation results of the chip formation process, the required time and RAM. The following geometric conditions for discretization of the chip formation zone were used:

- the FEM method uses division into 50,000 spatial, tetrahedral elements of size 9 μm and 30,000 nodes, as well as adaptive mesh change (remeshing),
- the EFG method uses the same conditions as FEM,
- in the SPH method the simulation zone was represented by 40,000 particles.

It can be seen from figures 2 and 3 that the FEM and EFG methods produce a similar chip shape, but the values of both maximum strains and reduced stresses are higher, i.e. ε_{max} = 3.3 and 6.3, and the corresponding stress values are σ_{max} = 1500 and 1750 MPa [9].

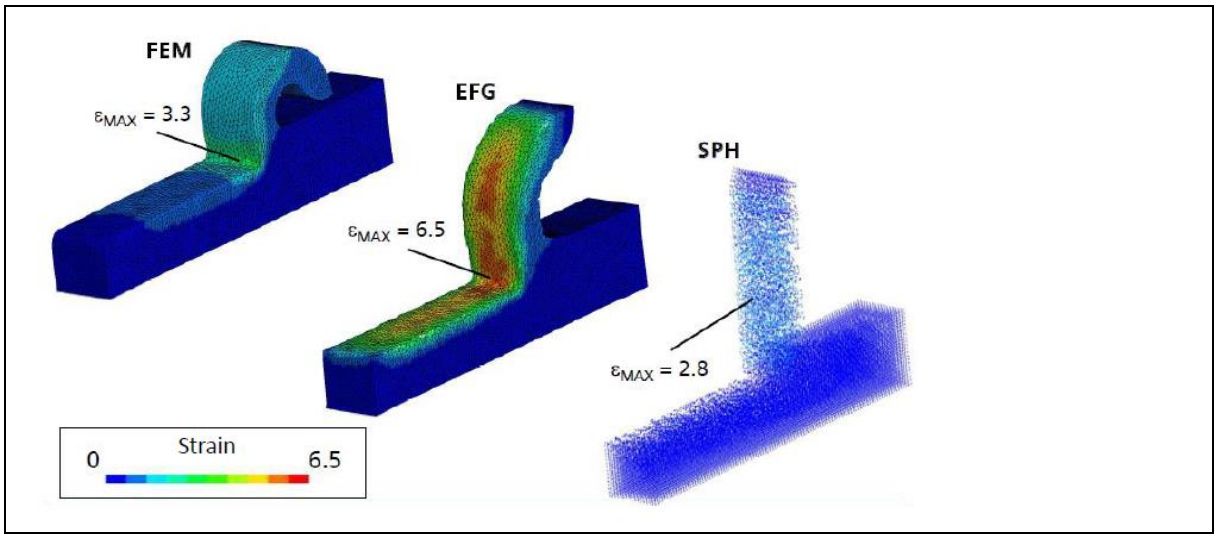

Fig. 3. Comparison of strain distribution in the chip formation zone using FEM, EFG and SPH methods [9]

In the SPH method, the determined values of strains and stresses are much smaller, i.e. ε_{max} = 2.8 (i.e. comparable to those in the FEM method) and σ_{max} = 980 MPa (i.e. comparable in the FEM and EFG methods). This may indicate that the simulation results strongly depend on the numerical conditions used in each of the methods, and in the SPH method on the kernel/smoothing function used.

It may be interesting for users to compare the computation times and the requirements for computational units. They are as follows (in the order FEM/FEG/SPH): computation time – 3:52/9:45/4:19 [h:min], volume of recorded data – 2320/2620/485 [MB], average RAM – 1.3/1.4/0.9 [GB]. These data speak in favour of the meshless method, especially with respect to the volume of collected data and the necessary RAM. The simplified preparation of the simulation model is also of great importance. Further reduction of simulation time is achieved in combined methods, which will be documented later in the article.

Comparative analysis of cutting process modelling and simulation results

In case of meshless modelling, friction is not taken into account, which is replaced by particle contact in the numerical approximation region. For this reason, an interesting problem is to compare the assumptions and simulation results of the SPH method and the hybrid SPH+FEM method, which was discussed in the previous article [1].

Since most of the studies using SPH simulations were carried out in the LS-Dyna package, fig. 4*a* shows a typical calculation cycle diagram, and fig. 4*b* presents the principle of selecting the location of neighbouring particles, which is important for obtaining information about which of the particles will try to contact other particles at any selected time of numerical calculations [11]. The calculation cycle is basically similar to the FEM method except for the steps in which the core approximation is used.

In fig. 4*b* the sphere of influence of each particle has a finite area of radius 2*h* (i.e. twice the smoothing length). The task of the neighbourhood search is to prepare a list of particles inside the domain at each time step of the simulation. For this purpose, an algorithm similar to the one used in the search for particle contact is used, the so-called search list – literally scooping with a bucket search. In this way, the search domain covered by particles is divided into several boxes as in fig. 4*b*. This approach significantly limits the number of determined distances and consequently shortens the computation time.

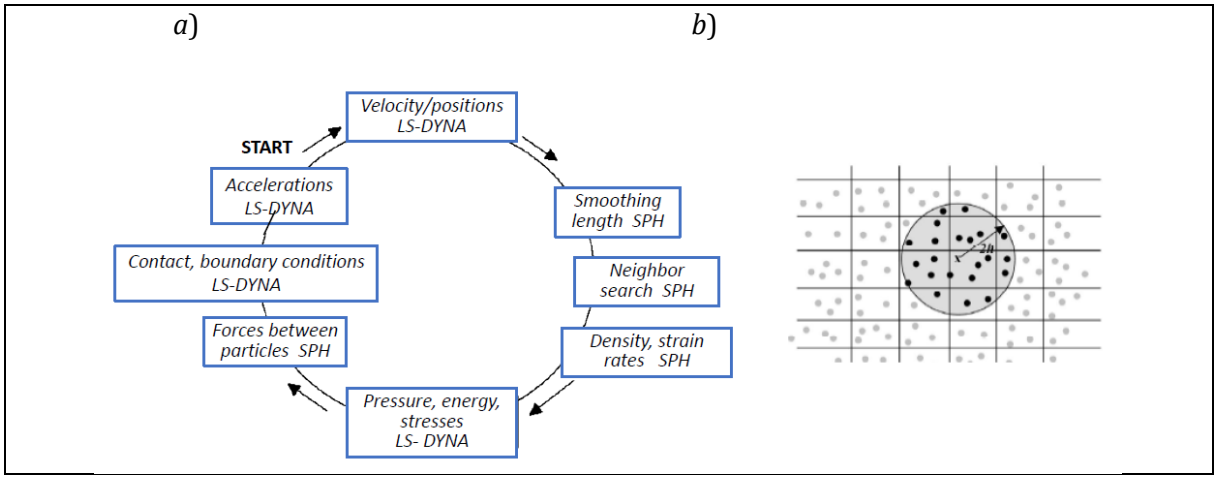

Fig. 4. Scheme of the calculation cycle in time for simulation using SPH method in LS-Dyna package (*a*) and a method of sorting and searching particles inside a finite domain (*b*) [10, 14, 18]

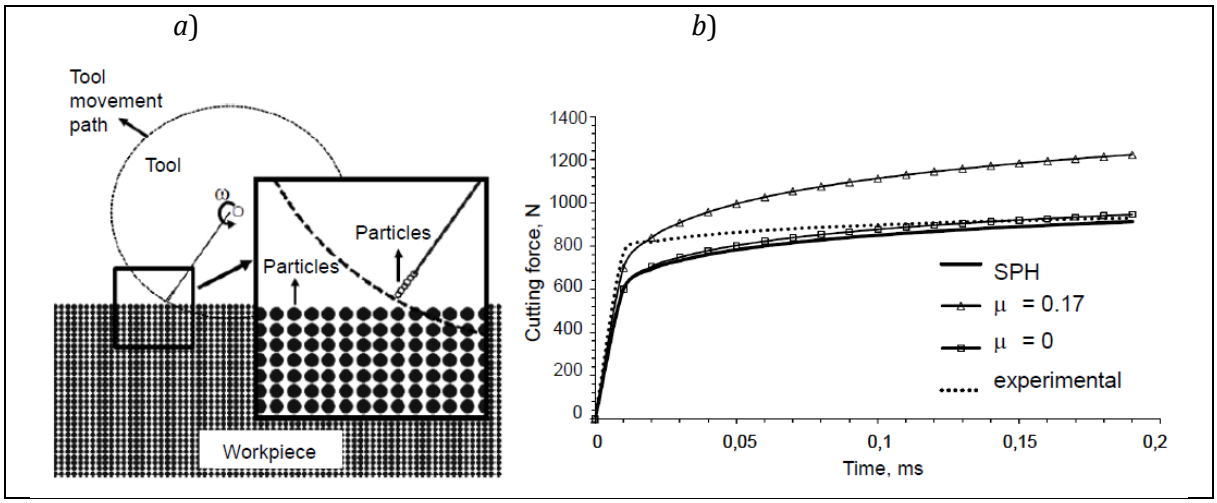

Fig. 5. Full SPH model of a rotational cutting process (*a*) and comparison of cutting force values determined in numerical simulations and obtained experimentally (*b*) [2, 6]

Figure 5*a* shows the configuration of the process model with the main rotary motion, e.g. cylindrical milling, in which the discretization of the tool and the workpiece was performed by particles, and fig. 5*b* shows a comparison of the cutting force values determined from the SPH simulation and the hybrid method (FEM for the tool and SPH for the workpiece) with the measurement results [10]. The machined material was an aluminium alloy of the A2024-T351 grade (Y = 400 MPa), and the machining conditions were as follows: v_c = 800 m/min, a_p = 0.1 mm, and f = 0.2 mm.

In the orthogonal FEM model carried out in the commercial package LS-Dyna, two values of the friction coefficient were assumed μ = 0 and 0.17, which in the first case corresponds to the interaction of neighbouring material particles (i.e. separation of the chip and the tool) assumed in the SPH model, and f = 4 mm/rev, a_p = 2 mm and the rake angle γ_0 = 17.5°. Figure 5*b* shows a good agreement of the

cutting force curve in time 0.2 ms for the SPH and FEM methods with the assumption of "frictionless" contact of the chip-cutting edge and the measurement result. It should be noted that the force values determined in the joint (SPH+FEM) model for $\mu = 0.17$ are already clearly higher, which is consistent with the information in the report [9]. This agreement depends on the phase of the process, i.e. in the first half, the force values determined by the SPH simulation method are clearly lower, which is the result of the characteristic fluctuation of the force value in time 0÷0.6 ms. In turn, the determined chip thickness and length are comparable.

The algorithm used in the study [10] allowed to determine the cutting and the passive force values with an accuracy of 8.4% and 12%. The EN AW6082-T6 aluminium alloy was cut at a speed of $v_c = 300$ m/min, feed rate $f = 0.234$ mm/rev and depth $a_p = 0.2$ mm. This was the result of the sensitivity analysis in relation to the resolution of the particle distribution, the mass of the particles, the duration of the process and the intensity of friction between the chip and the tool – the static and dynamic coefficients of friction were considered. The particle distribution density was assumed to be 512,000 particles/cm^3, the static and dynamic coefficient of friction was 0.23 and the calculation time was 31 h 43 min. The simulation result is illustrated in fig. 6.

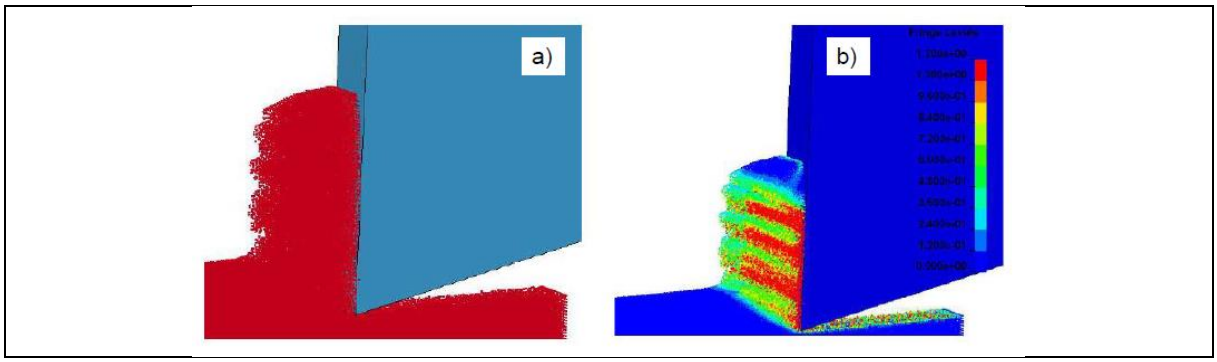

Fig. 6. The result of chip formation simulation using SPH method for the workpiece and FEM for the tool: *a*) 3D view and *b*) contours of effective plastic strain in the cutting zone [10]

Other studies, e.g. [10–13] have shown that the accuracy of force and deformation prediction without such analysis is much lower. For example, for the SPH/SPH method using the same simulation package, a 10% deviation was obtained for the cutting force and almost 30% for the passive force, which is consistent with the common knowledge in the field of cutting process simulation [6]. On the other hand, a comparison of the simulation time of cutting an aluminium alloy of grade 1100 Al using the FEM Euler and SPH methods shows that the corresponding maximum values of the shear strain are equal to 7.5 and 8, and the computation time on the CPU can be even 2.75 times shorter in favour of the SPH method [12]. The width of the primary deformation zone (PDZ) from fig. 6*b* was equal to 700 μm for the Euler model, 600 μm for the SPH model and 800 μm from the metallographic analysis, and the secondary deformation zone (SDZ) for the numerical models was approximately 250 μm.

Figures 7*a*–*d* presents a comparison of the plastic strain intensity distribution for four simulation methods: ESPH, TLSPH, MPM (material point method) and FEM [13]. Two meshless methods were used, namely ESPH (Eulerian SPH) and TLSPH (total lagrangian SPH), in which a special procedure for determining the smoothing function in the reference configuration was used and the possibility of describing the mutual interaction and penetration of particles during their contact was introduced. Therefore, the Eulerian and Lagrangian smoothing cores were distinguished. In this way, simulation instabilities leading to numerical material fracture were eliminated. The simulation results were verified using the Taylor test [6]. AISI 4340 steel was cut orthogonally at a speed of 50 m/s. It was found that the simulation results of the chip formation and slip bands in the chip obtained by the ESPH and TLSPH methods (fig. 7*a* and *b*) are similar to the results obtained by the MPM method and the classical FEM method (fig. 7*c* and *d*), but in favour of the TLSPH method. This situation results, as indicated above, from the significant elimination of instability. The TLSPH simulation better represents the chip curvature (fig. 7*b*). There is also no need to regulate the unit pressures. The simulations were carried out in the LS-Dyna package.

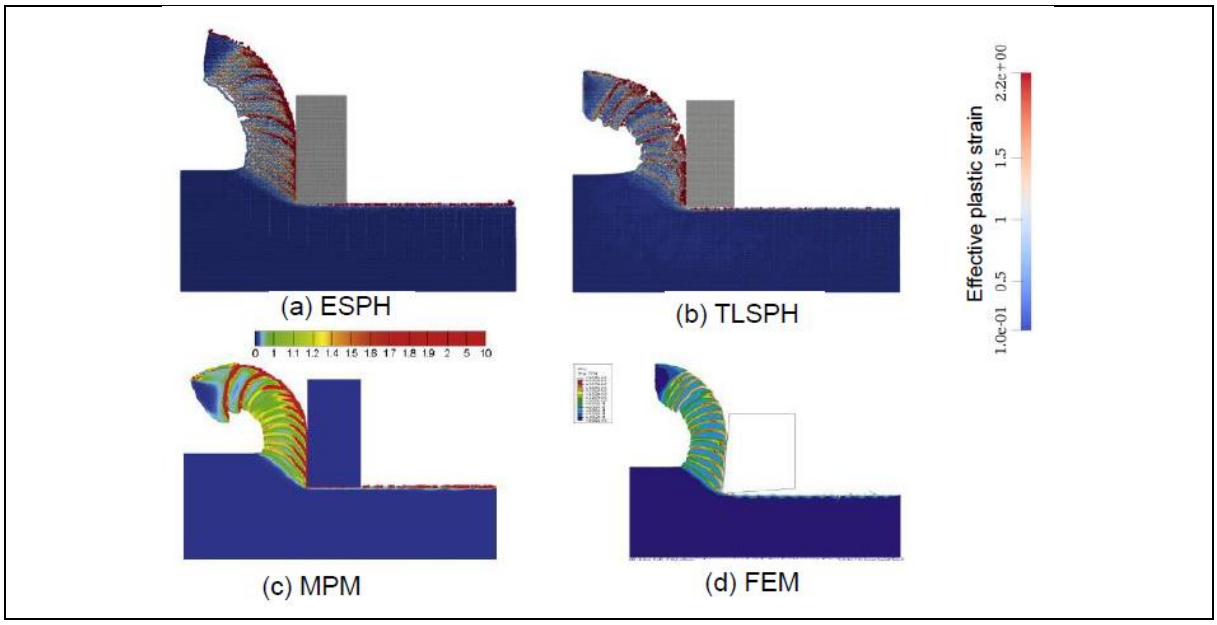

Fig. 7. Comparison of distribution of effective plastic strain using four simulation methods of metal cutting process, i.e.: ESPH, TLSPH, MPM and FEM [13]

As mentioned previously [1], hybrid models of the (SPH+FEM) type are being developed, which increase the accuracy of the prediction of process characteristics and contribute to a significant reduction of the computational time. In such a case, the SPH model concerns only a severe deformed layer separated from the rest of the material, and the rigid tool is subject to discretization with a FEM mesh. The basic problem is the numerical connection of particles and FEM mesh elements and the selection of the damage parameter D in the constitutive equation [6]. Then, the number of particles in the SPH model can be reduced by up to 50%. For this reason, in the work [14], almost 40% reduction of the computational time of both 3D orthogonal cutting and micro-cutting with a depth of 300 μm was documented. The similarity in the simulation result using both methods is confirmed by the predicted cutting force values equal to 15 N and 15.1 N, respectively. In turn, the simulation time was shortened by 43%.

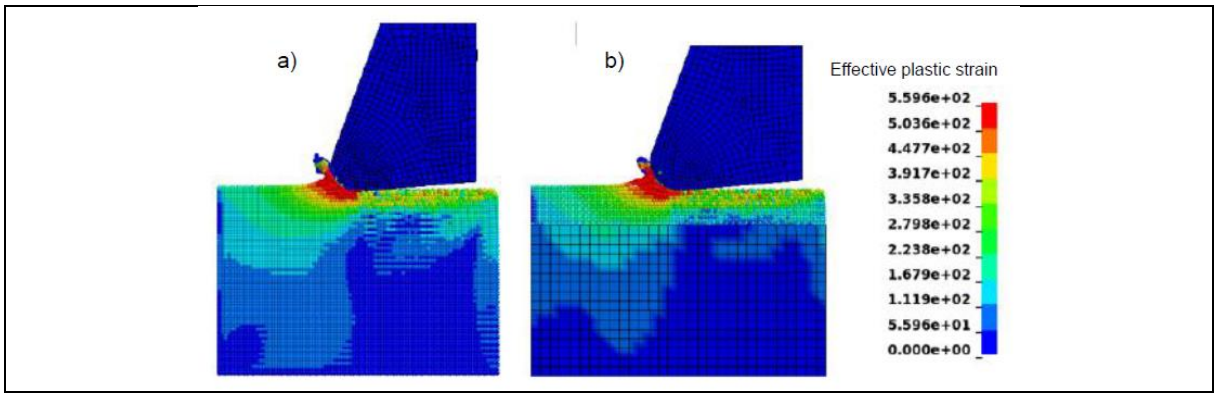

Fig. 8. Distributions of the effective von Mises stresses in *a*) orthogonal and *b*) oblique machining determined by using SPH model [30]

Figure 8 shows the distributions of the reduced von Mises stress for orthogonal (2D) and oblique (3D) cutting obtained from SPH simulations [30]. A new approach to the analysis of SPH simulation results is the use of machine learning (ML) [21]. In this case, the DOE (design of experiment) method [22] and an artificial neural network were used to assess the effect of cutting parameters (r_β, f, v_c, γ_0) on the cutting force components and specific forces (k_c, k_f) in orthogonal cutting of Ti6Al4V titanium alloy. The relationships were obtained in accordance with the experimental and literature data [6].

Thermal simulation and wear evolution

The previously discussed TLSPH method is also useful for thermal analyses in that the temperature distribution is determined based on its correspondence to the equivalent plastic strain distribution [6, 13].

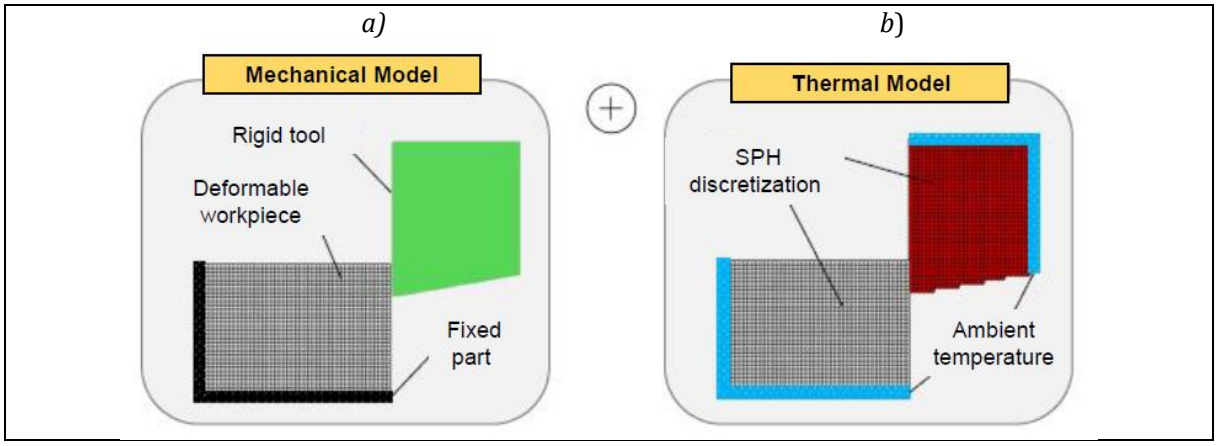

Fig. 9. Configuration of the thermomechanical SPH model: *a*) initial geometry and *b*) boundary conditions [17]

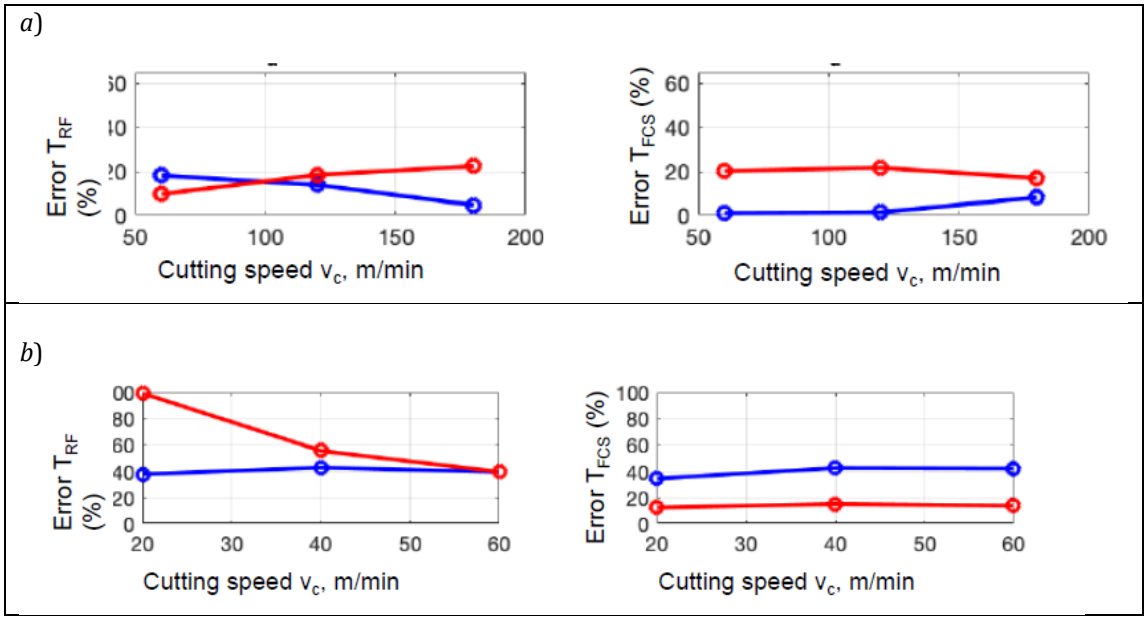

Fig. 10. Temperature prediction errors at the rake face and free chip surface by means of SPH and PEFM models in orthogonal machining of *a*) AISI 1045 steel and *b*) titanium alloy Ti6Al4V (b) [17]

Figure 9 shows the original concept of a thermo-mechanical model with SPH discretization for the workpiece material and the cutting edge to simulate the orthogonal cutting process. As in many models of this type, the tool is a perfectly rigid element and the workpiece is a deformable element. It was assumed that the SPH particles are not active on the contact side of the cutting edge. In order to include the effect of heat in the initial model (fig. 9*a*), the appropriate equations describing heat generation in cutting are solved [6]. The discretization of the workpiece with SPH particles (fig. 9*b*) is performed on an area of 3 mm length and width equal to at least three times the chip thickness. The smoothing parameter was assumed equal to h = 1.3 Δx (Δx is the distance between particles).

Figure 10 shows the determined errors of the temperature prediction on the rake face (T_{RF}) and the free chip surface (T_{FCS}) in the SPH and PEFM (particle FEM – Lagrangian technique for modelling the motion of nodes/particles) methods [18, 19] in orthogonal cutting of AISI 1045 steel (*a*) and Ti6Al4V titanium alloy (*b*) for the cutting layer thickness h = 0.15 mm compared to the measured values. They depend on the measurement location, the type of workpiece, the undeformed chip thickness (h) and the cutting speed (v_c) and are within 20÷40% except for the cases of low speeds. Generally, the temperature predictions on the rake face are more accurate for AISI 1045 steel than for Ti6Al4V titanium alloy. On the other hand, the SPH method gives a better agreement for the temperature on the free chip surface for the titanium alloy.

The SPH simulation proved to be useful for the evaluation of the wear of the 4÷8 μm thick outer layer of CVD-Al_2O_3/TiCN coating in the cutting of pearlitic-ferritic steel grades 45R (P75/F25) and 60R (P85/F15) [28]. The SPH model of the workpiece contained 18,000 SPH particles, which corresponds to the density of 4.5×10^6 particles/cm^3. Figure 11*a* shows the predicted increase in the width of the top coating abrasion, which corresponds well with the SEM studies.

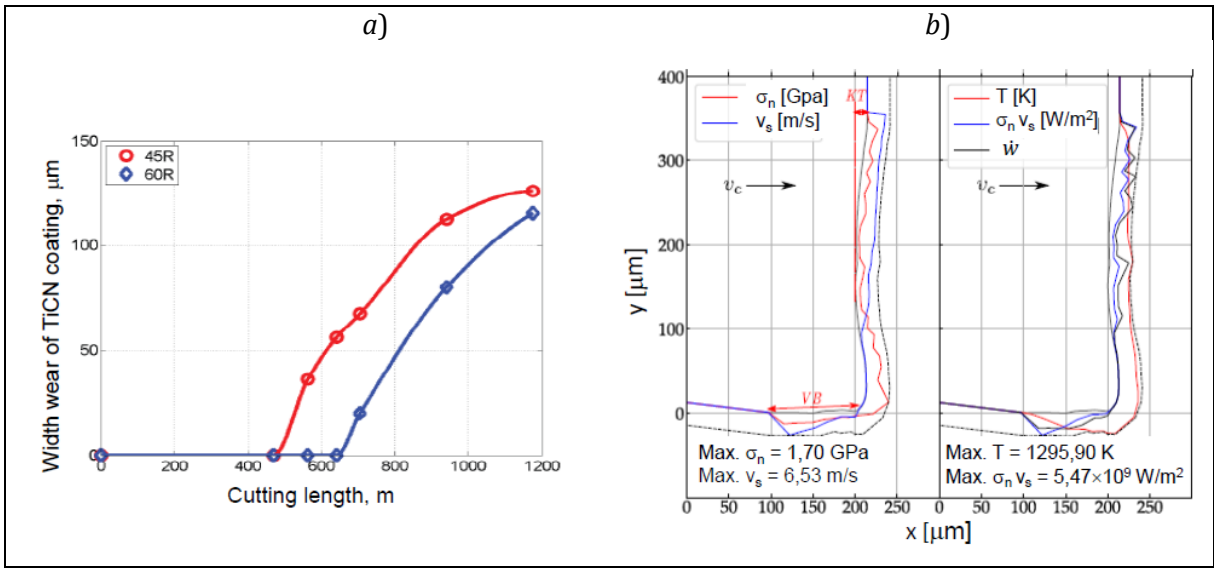

Fig. 11. Progress of the width of exposed TiCN coating as a function of the cutting length [28] (*a*) and simulated thermo-mechanical conditions and wear rates on the tool-chip and tool-workpiece contacts (*b*) [29]

In the work [29], the workpiece (tool) model contained 419,000 SPH particles. Figure 11*b* shows the predicted distributions of thermo-mechanical conditions and cross-sections of wear traces on the rake face (KT) and flank face (VB_B) at the moment when $VB_B \approx 100$ μm. It can be observed that the match between the measurement curves and the predictions is not perfect because abrasive wear is taken into account while diffusion wear is omitted.

Simulation of abrasive and hybrid abrasive assisted machining

The simulation of the abrasive machining process is based on the use of the results of the orthogonal cutting test (2D) and scratch test (3D) and then modelling the scratch trace (groove and side flashes) [22] using the PFEM (particle FEM method) and SPH [23] methods. The discretization of such models is illustrated in fig. 12*a*. Particles with a diameter of d_p = 3 μm and the same FEM mesh element were used in the comparative ALE method. The simulation was performed in the ABAQUS Explicit 2019 package.

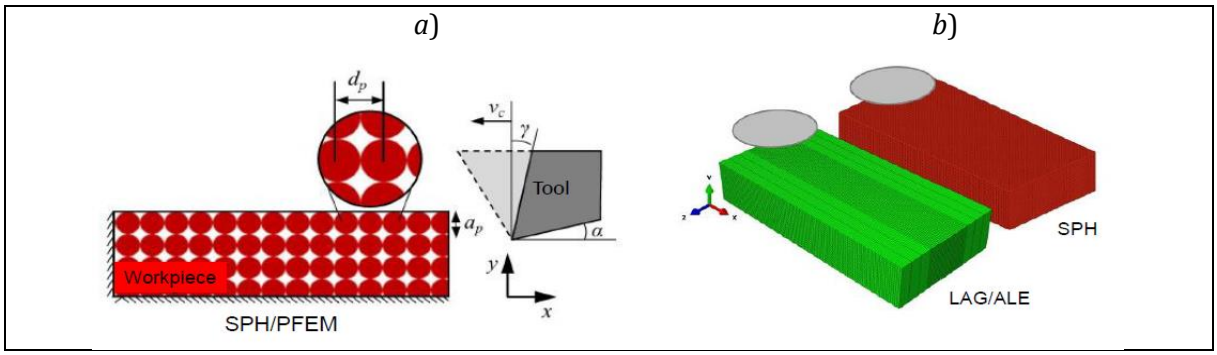

Fig. 12. Configuration and discretization of SPH/PFEM models in the analysis of *a*) orthogonal cutting and *b*) scratch test [23]

Figure 13 shows a comparison of the reduced stress distributions (*a*) and cutting force values (*b*) using mesh and meshless methods. The results refer to the scratch test with a conical aperture angle of 105° and a depth of a_p = 50 μm. Figure 13*b* clearly shows that the underestimation of the component forces reaches even 40÷60%. In turn, classical grid methods give results that differ from the measurements by about 10%. They undoubtedly prove that the scratch test results cannot be related to 2D models.

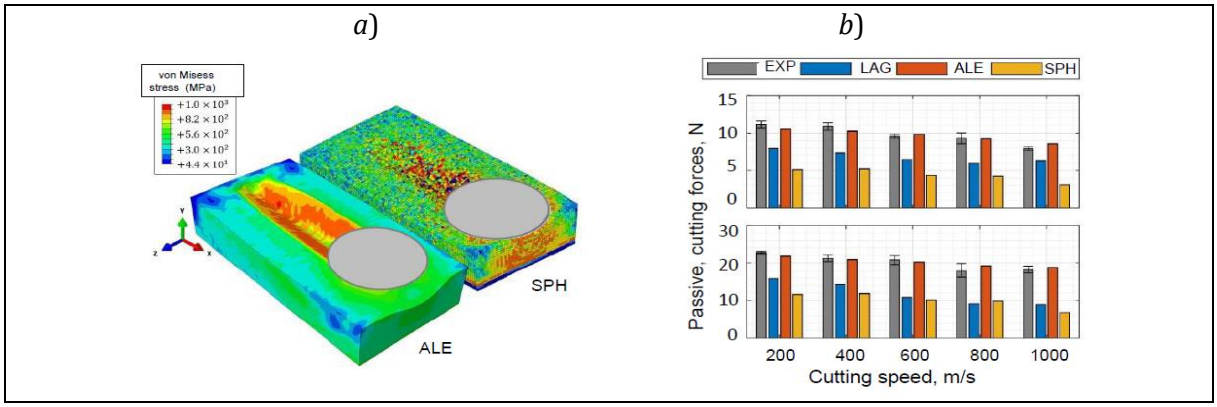

Fig. 13. Distribution of effective von Mises stress determined in ALE and SPH simulation methods (*a*) and predicted values of cutting forces (*b*) [23]

In the article [24] an SPH simulation package called iMFREE was presented, which, in addition to the simulation of typical orthogonal cutting, can also be used for single-grain and multi-grain grinding of the titanium alloy Ti6Al4V and silicon carbide SiC. Figure 14*a* shows the result of the simulation of simultaneous cutting of five grains of the titanium alloy Ti6Al4V (*a*), and fig. 14*b* shows the result of the simulation of silicon ceramics with visualization of hydrostatic stress distribution and scratch marks.

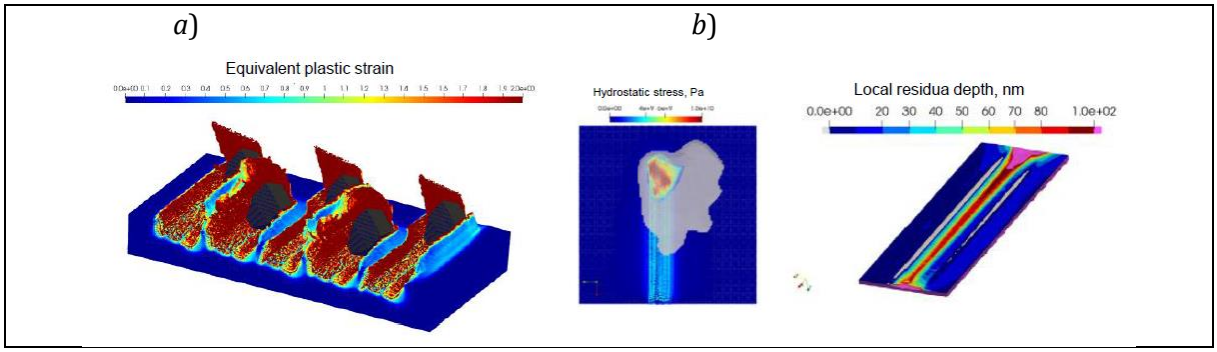

Fig. 14. Result of concurrent grinding with 5 diamond grains titanium alloy Ti6Al4V (*a*) and silicon ceramics with visualization of hydrostatic stress and scratching grooves (*b*) [24]

It has been proven that the simulation in the iMFREE package speeds up the simulation time by 90 times (normal simulation takes 90 hours) and well represents the interaction of neighbouring grains in the grinding wheel in the real process with very high resolution (fig. 14*a*). In turn, fig. 14*b* shows the 3D simulation cutting with diamond grain in a plastic state with visualization of the hydrostatic stress distribution and the effect of elastic recovery, which changes the scratch depth after the grain passes compared to an initial penetration of 500 μm.

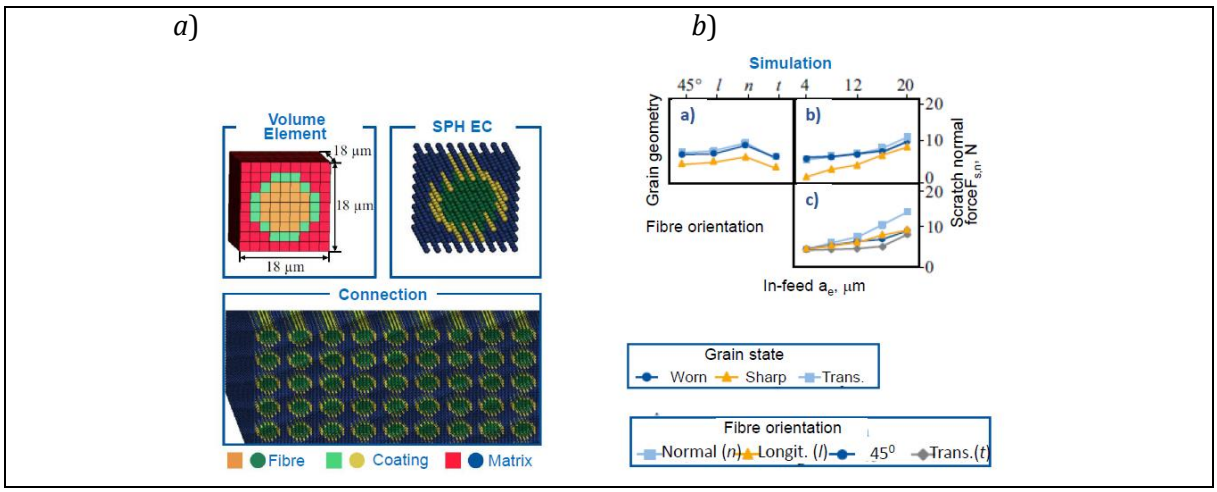

Fig. 15. SPH modeling and discretization of SiC/SiC ceramics (*a*) and influence of grain geometry, infeed and fiber orientation on the value of scratching normal force (*b*) [25]

In the article [25] a method of using SPH simulation for the analysis of single-grain grinding of two two-phase ceramic materials – WC-12%Co sintered carbide and SiC/SiC reinforced with SiC fibers – was presented in the scope of predicting the normal force. The influence of the abrasive grain condition was considered, infeed and fiber direction.

Figure 15*a* shows the method of modelling the structure of the object by combining a spatial element with separated boxes and elementary cells (EC – elementary cell) filled with particles imitating SiC fibers, which are 2 μm apart. Each cell contains 729 particles, which, with the assumed dimensions of the ceramic object 16/16/6 (length/width/height) EC, gives a total number of particles equal to 1119744 in the scratch simulation and prediction of the normal force $F_{s,n}$. Similarly to the previous examples, large discrepancies were demonstrated between the simulation and measurement results, especially for the infeed above 8 μm (fig. 15*b*). They are caused by the change in grain geometry due to wear, i.e. in reality the grain is not sharp but in a state of partial wear (hybrid). In the studies of the scratch surface morphology, areas of the plastic and brittle state were distinguished [6].

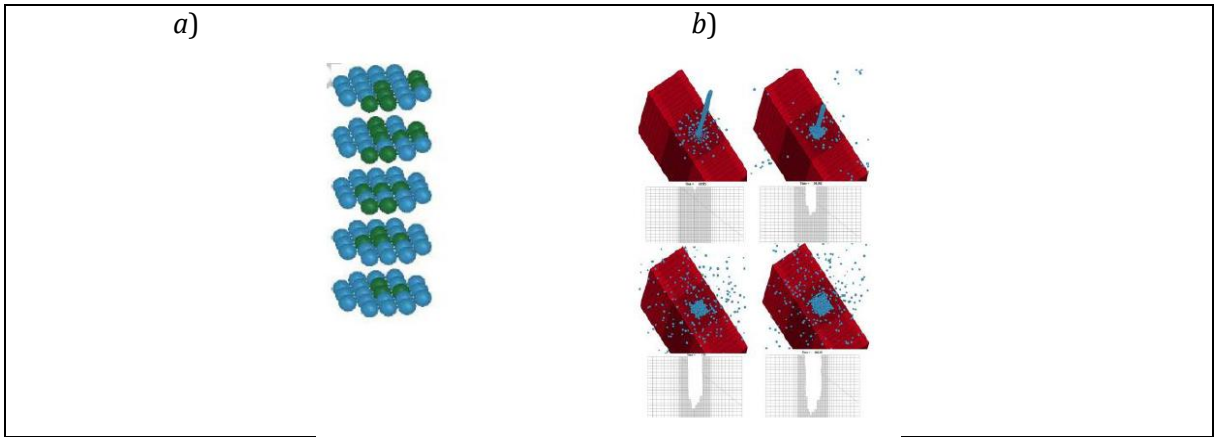

Fig. 16. Distribution of the abrasive and water SPH particles (*a*) and simulation of the cross-section evolution at different time intervals (*b*) [26]

Due to the nature of the process, water-abrasive jet cutting is a very good example of the use of SPH simulation. The number of particles in the SPH model of the water-abrasive suspension was determined based on their percentage content and the mass flow rate. For example, the model is made up of 2340 water particles and 58 abrasive particles. Their distribution was determined randomly as in fig. 16a. The model of the workpiece with dimensions 30 × 1 × 55 mm was made of low-carbon steel. The jet pressure was equal to 100 MPa. The development of the groove in time is illustrated in fig. 16*b*. The simulation was carried out in the LS-Dyna program.

Due to the long simulation time, a better solution is to combine the SPH method with DEM (discrete element method*)* [27] where the discretization of the water jet and the workpiece is performed using SPH particles, and each abrasive grain is modelled as a DEM particle. SPH and DEM particles are combined based on the calculated interaction forces between these phases and related to the local porosity of the water-abrasive jet. The basic aspect is the simulation of a single impact of the water-abrasive jet on the free surface of a solid body. As a result, a visualization of the evolution of the impact of the water-abrasive jet on the free surface of an OFHC copper element with visible plastic deformations and small local indentations (micro-craters) is presented. The simulation was performed in 60,000 times steps for 840 s [27].

Composite Material Processing Simulation

An interesting application of the coupled SPH+FEM method is the simulation of CFRP (carbon fibre reinforced plastic) composite cutting, where the destruction of carbon fibres and polymer matrix is separated [15]. In this model, the mesh openings are arranged along the fibres, and in the centre of each of them an SPH particle with a diameter of 0.7 μm is placed, which causes it to become active if the material decohesion is initiated.

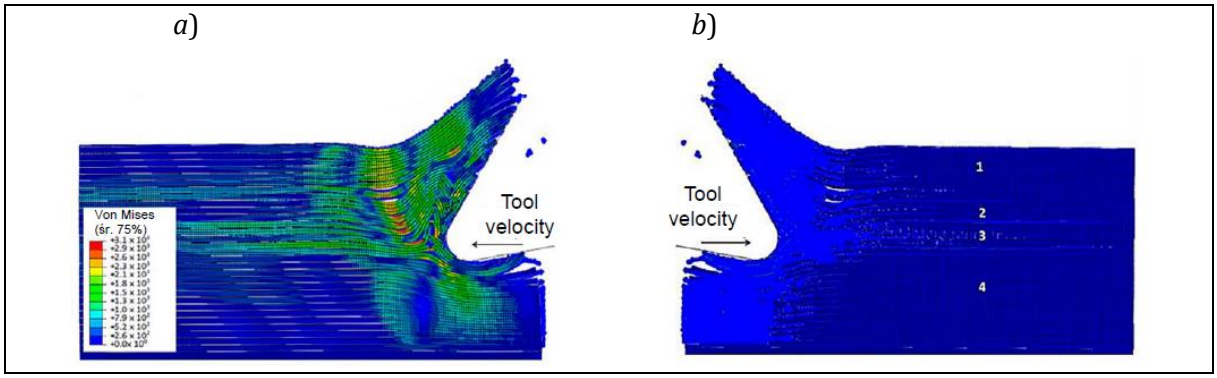

Fig. 17. FEM-SPH model configuration at 2.85 × 10^{-3} s for the fiber orientation and a matrix damage of *D* = 0.8: *a*) fiber section, *b*) matrix section [15]

It can be observed in fig. 17*a* that during cutting a crack appears which moves perpendicularly to the cutting edge towards the workpiece surface. This effect is caused by several mechanisms, namely that the crack initiation at the blade end is the result of fiber buckling and its propagation is due to the crack due to bending. The model indicates that the matrix material under the blade is compressed leading to visible deformation of the particles which are squeezed outwards. Similar to the FEM model, there is an agglomeration of broken fibers and matrix particles, but this effect is more visible. The area located at the tool end (fig. 17*b*) can be divided into 4 separate ribbons/bands of which bands 1 and 4 experience fiber bending and 2 and 3 essentially undergo buckling. Additionally, due to the tool movement, SPH particles accumulate around the cutting edge.

Summary

Meshless SPH or hybrid simulation methods (SPH-FEM, SPH-DEM) are a promising tool for numerical solutions in subtractive machining processes, including chip formation, mechanical and thermal

characterization of the chip formation zone in cutting and grinding, tool wear, the interaction of abrasive grains and water-abrasive suspension in AWJM machining, or fiber interactions in machining of CFRP composites. They contribute to the inclusion of complex physical mechanisms in simulations and the visualization of the 2D and 3D process. Modules are available in popular simulation packages, e.g. LS-Dyna or proprietary programs, e.g. described in [24]. Detailed descriptions of the modelling basics and the procedures used can be found in the appropriate literature.

REFERENCES

[1] Grzesik W. "Progress in modelling and simulation of the machining process – part I: Multiscale modeling" / „Postęp w modelowaniu i symulacji procesu skrawania – część I: Modelowanie wieloskalowe". *Mechanik*. 3 (2024): 30–37, https://doi.org/10.17814/mechanik.2024.3.4.

[2] Zhang N., Klippel H., Afrasiabi M., Röthlin M., Kuffa M., Bambach M., Wegener K. „Hybrid SPH – FEM solver for metal cutting simulations on the GPU including thermal contact modelling". *CIRP Journal of Manufacturing Science and Technology*. 41 (2023): 311–327, https://doi.org/10.1016/j.j.cirpj.2022.12.012.

[3] Yanagimoto J., Banabic D., Banu M., Madej L. "Simulation of metal forming. Visualization of invisible phenomena in the digital era". *CIRP Annals – Manufacturing Technology*. 71 (2022): 599–622, https://doi.org/10.1016/j.cirp.2022.05.007.

[4] Zhang Y., Jung Y-G, Zhang J. "*Multiscale modelling of additively manufactured metals".* Elsevier (2020).

[5] Rojek J. „Modelowanie i symulacja komputerowa złożonych zagadnień mechaniki nieliniowej metodami elementów skończonych i dyskretnych". *Prace IPPT PAN.* 4 (2007), https://rcin.org.pl/Content/67301/PDF/WA727_16636_4-2007_Rojek-Modelowanie.pdf.

[6] Grzesik W. „*Podstawy skrawania materiałów konstrukcyjnych".* Warszawa: PWN (2018).

[7] Orkisz J. „Dziś i jutro metod komputerowych mechaniki", https://kmech.pan.pl/images/stories/prezentacje/50lecieKM/metody%20komputerowe%20mechaniki.pdf (dostęp: luty 2024).

[8] Danielewicz A. „Metoda SPH+MES na przykładzie symulacji wzmocnienia podłoża gruntowego metodą wymiany dynamicznej". *Rozprawy i Monografie PG*. Gdańsk: Politechnika Gdańska (2016).

[9] Martinez H.V. "Practical comparison between the finite-element and mesh-free calculation methods in the analysis of machining simulations". Fraunhofer IPA, https://www.dynamore.de/de/download/papers/dynamore/de/download/papers/2014-ls-dyna-forum/documents/simulationsmethodik-ii/practical-comparison-between-the-finite-element-and-mesh-free-calculation-methods-in-the-analysis-of-machining-simulations (dostęp: luty 2024).

[10] Villumsen M.F., Fauerholdt T.B. "Simulation of metal cutting using Smooth Particles Hydrodynamics". *LS-Dyna Anwenderforum*, Sektion Metallumformung III. Bamberg (2008).

[11] Dehghani M., Shafiei A. "Replacing friction model with interaction between particles in analyzing orthogonal and rotational cutting processes using SPH method". *Journal of Computational Applied Mechanics.* 52(2) (2021): 297–306, https://doi.org/10.22059/jcamech.2019.280356.390.

[12] Akarca S.S., Altenhof W.J., Alpas A.T. "A Smoothed-Particle Hydrodynamics (SPH) model for the machining of 1100 aluminium". *10th International LS-Dyna® Users Conference*, Section Metal Forming. 3 (2008): 12.1–12.8, https://www.dynalook.com/conferences/international-conf-2008/MetalForming3-1.pdf.

[13] Islam R.I., Bansal A., Peng Ch. "Numerical simulation of metal machining process with Eulerian and Total Lagrangian SPH". *Engineering Analysis with Boundary Elements*. 117, 5 (2020): 269–283, https://doi.org/10.1016/j.enganabound.2020.05.007.

[14] Ojal N., Cherukuri H.P., Schmitz T.L., Jaycox A.W. "A comparison of smoothed particle hydrodynamics (SPH) and coupled SPH-FEM methods for modeling machining". *Proceedings of the ASME 2020 International Mechanical Engineering Congress and Exposition*, IMECE2020-24646 (2020), https://doi.org/10.3390/jmmp6020033.

[15] Abena A., Ataya S., Hassanin H., El-Sayed M.A., Ahmadein M., Alsaleh N.A., Ahmed M.Z., Essa K. "Hybrid Finite Element-Smoothed Particle Hydrodynamics Modelling for Optimizing Cutting Parameters in CFRP Composites". *Polymers*. 15, 2789 (2023), https://doi.org/10.3390/polym15132789.
[16] Nguyen T.T., Hojny M. "Application of Smoothed Particle Hydrodynamics Method in Metal Processing: An Overview". *Archives of Foundry Engineering*. 2022, 3 (2022), https://doi.org.10.24425/afe.2022.140238.
[17] Prieto J.M.R., Larsson S., Afrasiabi M. "Thermomechanical Simulation of Orthogonal Metal Cutting with PFEM and SPH Using a Temperature-Dependent Friction Coefficient: A Comparative Study". *Materials*. 16, 3702 (2023), https://doi.org/10.3390/ma16103702.
[18] Limido J., Espinosa C., Salaun M., Lacome J.L. "SPH method to high speed cutting modelling". *Int. J. Mechanical Sciences.* 49 (2007): 898–908, https://doi.org/10.1016/j.ijmecsci.2006.11.005.
[19] Markopoulos A.P., Karkalos N.E.,· Papazoglou E.-L. "Meshless methods for the simulation of machining and micro-machining: A review". *Archives of Computational Methods in Engineering*. 27 (2020): 831–853, https://doi.org/10.1007/s11831-019-09333-z.
[20] Fraser K.A., St-Georges L., Kiss L.I., Chiricota Y. "Hybrid Thermo-Mechanical Contact Algorithm for 3D SPH-FEM Multi-Physics Simulations". *IV International Conference on Particle-Based Methods – Fundamentals and Applications – Particles 2015*. E. Oñate, M. Bischoff, D.R.J. Owen, P. Wriggers & T. Zohdi (Eds). Barcelona (2015).
[21] Klippel H., Sanchez E.G., Isabel M., Röthlin M., Afrasiabi M., Kuffa M., Wegener K. "Cutting force prediction of ti6al4v using a machine learning model of SPH orthogonal cutting process simulations". *Journal of Machine Engineering*. 22, 1 (2022): 111–123, https://doi.org/10.36897/jme/147201.
[22] Grzesik W., Żak K., Tomkiewicz-Zawada A. *Analiza i modelowanie powierzchni wytwarzanych w obróbce ubytkowej.* Warszawa: PWN, 2023.
[23] Sridhar P., Prieto J.M., de Payerebrune K.M. "Modeling grinding processes – mesh or mesh-free methods, 2D or 3D approach?". *J. Manuf. Mater. Proc*. 6, 120 (2022), https://doi.org/10.3390/jmmp60500120.
[24] Klippel H., Zhang N., Kuffa M., Afrasiabi M., Bambach M., Wegener K. "iMFREE: A versatile software tool for modelling machining process with particle methods". *Procedia CIRP*. 117 (2023): 13–19, https://doi.org/10.1016/j.procir.2023.03.004.
[25] Dehmer A., Prinz S., Breurer P., Barth S., Bergs T. "Simulation of machining behaviour of two-phase brittle materials during grinding by modelling single-grain scratching using a combination of FE and SPH methods". *Int. J. Advance Manufacturing Technology*. 128 (2023): 1709–1723, https://doi.org/10.1007/s00170-023-12006-8.
[26] Shahveri H., Zohoor M., Mousavi S.M. "Numerical simulation of abrasive water jet cutting process using the SPH and ALE methods" *Int. J. Advanced Design and Manufacturing Technology*. 5/1 (2011): 43–50.
[27] Yu R., Dong X., Li Z. "A coupled SPH-DEM model for the simulation of abrasive water-jet impacting solid surface". ICCM Conferences. *The 13th International Conference on Computational Methods* (ICCM2022). *Computational Practicle Mechanics*. 10 (2023): 1093–1112, https://doi.org/10.1007/s40571-023-00555-4.
[28] Stenberg N., Delic A., Björk T. "Using the SPH method to easier predict wear in machining". *Procedia CIRP*, 58 (2017): 317–322, https://doi.org/10.1016/j.procir.2017.03.234.
[29] Zhang N., Klippel H., Kneubühler F., Afrasiabi M., Röthlin M., Kuffa M., Bambach M., Wegener K. "Study on the effect of wear models in tool wear simulation using hybrid SPH-FEM method". *Procedia CIRP*. 117 (2023), 414–419, https://doi.org/10.1016/j.procir.2023.03.070.
[30] Spreng F., Eberhard P. „Machining process simulations with Smoothed Particle Hydrodynamics". *Procedia CIRP*. 31 (2015): 94–99, https://doi.org/10.1016/j.procir.2015.03.073.